Luo, S., Ibraim, E., & Diambra, A. (2019). Acoustic Emission monitoring of crushing of an analogue granular material. *Géotechnique Letters*, *9*(4), 305–313. https://doi.org/10.1680/jgele.18.00231

Acoustic Emission monitoring of crushing of an analogue granular material

Sha Luo
University of Birmingham, Birmingham, UK
Formerly Department of Civil Engineering, University of Bristol, Bristol, UK

E Ibraim
Department of Civil Engineering, University of Bristol, Bristol, UK,
http://orcid.org/0000-0003-1077-0546

A Diambra
Department of Civil Engineering, University of Bristol, Bristol, UK
http://orcid.org/0000-0003-4618-8195

Corresponding author:
E Ibraim
Civil Engineering Department
Faculty of Engineering
University of Bristol
Queens Building, Room 2.35
University Walk
Bristol BS8 1TR
0117 3315734
erdin.ibraim@bristol.ac.uk

Themed Issue: Latest findings on Micro to Macro Mechanics of Geomaterials

Abstract

A two-dimensional analogue material formed of rod cylinders of chalk is tested under one-dimensional oedometric loading conditions. Passive non-destructive Acoustic Emission (AE) monitoring technique is used to document the occurrence of crushing of individual particles. While the AE activity is recorded by a sensor placed on the sample boundaries, the AE signals are also corroborated with the observations based on video records of the exposed face of the 2D sample, as well as vertical loading and displacement measurements of the global sample. In the process, one-dimensional tests on individual cylindrical rods were also conducted and their AE crushing signatures compared with the AE data recorded at the 2D sample scale. While AE signal features can capture the particle crushing in the 2D granular systems, their occurrence shows high complexities driven by internal crushing particle mechanisms and geometrical position of particles with respect to the AE monitoring device. The frequency content of AE signals shows some evidence of the existence of an AE signature for a typical particle crushing mechanism, which may be a consequence of the dynamic properties of the whole system.

Keywords

Laboratory tests; Monitoring; Particle crushing; Analogue soil

Introduction

Granular soils subjected to mechanical loading may experience grain crushing (White and Bolton, 2004; Muir Wood, 2007; Lackenby et al., 2007; Indraratna et al., 2009; Kuwajima et al., 2009). The progressive changes in the grading have significant consequences for the behaviour of granular soils (stress-strain, strength, volumetric response, hydraulic conductivity). However, its correlation with standard soil mechanics parameters are still problematic.

This paper explores the prospect of using passive non-destructive Acoustic Emission (AE) monitoring technique to document the occurrence of crushing of individual particles in an unbounded granular soil under loading. The acoustic emissions are micro-seismic events that occur in the material during loading. The AE data, normally recorded by an array of transducers, can complement other mechanical measurements of stress and strain, potentially providing insight into various internal particle phenomena. AE technique has been used in the monitoring of various engineering materials and applications (Dai and Labuz, 1997; Yuyama et al., 1994; Giordano et al., 1998; Bohse, 2000; Huguet, 2002; Haselbach, 2003; Shigeishi et al., 2001; Stojanova et al., 2014, among others). In geomechanics, pioneering work by Koerner and Lord (1974), (1976), (1977), Lord and Koerner (1974) established that laboratory testing of small-scale soil samples generates measurable AE signals the cumulative signal features of which correlate well with the stress response. These results paved the way for the use of AE in field monitoring of dams (Lord and Koerner,1975), deep excavations (Young and Martin, 1993), and slopes (Chichibu et al., 1989; Dixon et al., 2003; Dixon and Spriggs, 2007; Smith et al., 2014). Correlations between the AE signal features and stress, deformation, volumetric and hydraulic conductivity characteristics of samples under various loading conditions have been explored by Tanimoto et al. (1981), (1986), Hung et al. (2009), Michlmayr and Or (2014) for unbounded and Wang et al. (2009), Zhang et al. (1990), Baud et al. (2004), Ingraham et al. (2013) for bounded granular soils. Analysis of grain crushing phenomena in relation to the AE was reported by Karner et al. (2003), Arslan and Baykal (2006), Fernandes et al. (2010) for samples under oedometer, direct shear and triaxial compression loading, while Mao and Towhata (2015), Luo et al. (2016a and b), (2018), Ibraim et al. (2017) studied single particles of various materials under uni-axial loading. In most of these studies the analysis of the AE information is reduced to

a counting process of the recorded AE events, including their features associated with the averaged quantities of the material response. Nevertheless, as the AE data is the result of a collection of (often simultaneous) internal particle-scale (micro-mechanical) processes - from particle sliding and rotation, fabric rearrangement, to particle crushing and bond breakage, among others - a more significant challenge would be the identification of the AE signature against these internal particle phenomena. The challenges increase if discrimination of various particle crushing mechanisms (abrasion, chipping, splitting) is sought from the AE information.

While the wider research question is whether the AE technique has the potential to infer the particle breakage in a soil mass under loading, supporting the prediction of its extent and evolution, the objective of this work is much more contained and limited to the study of particle breakage in a simpler two-dimensional analogue granular system. As the complexity of the granular system is gradually increased, from one particle to multi-particles, the connections between the grain crushing mechanisms and the related AE features are explored together with the systemic effect of the AE crushing-type signature.

2. Material and experimental set up

A granular analogue material comprising of cylindrical rods was considered and tested under one-dimensional compression. Two-dimensional (2D) analogue granular systems, rods or disks, were used to study the internal particle kinetics, fabric and microstructure evolution under loading and to check various constitutive soil model conjectures (Mogami, 1965; Calvetti et al., 1997; Takei et al., 2001; Geng and Behringer, 2005; Wan et al., 2005; Ibraim et al., 2010; Misra and Poorsolhjouy, 2013). In this study, the 2D system provides visual access to one side of the sample allowing a direct correlation between the particle crushing occurences and the AE events. Commercial stationery blackboard chalk (fine crushed quarried limestone mixed with water in a slurry, extruded through a die and cured in an oven) 9 mm diameter cylinders cut to 9 mm length size, were used as rod material (density of 715 kg/m^3). The advantages of using such material are their low breakage point force demand and the less explosive nature of their breakage mechanism. Progressive crushing of chalk cylinders in 2D samples has also been studied by Tsoungui et al. (1999), Takei et al. (2001) and Liu (2010).

A series of oedometer tests on 2D assemblies was designed (Figure 1a), including: laterally confined tests on single chalk cylinders (R1) and 2D single column samples comprising two (R2), three (R3), four (R4) and five (R5) chalk cylinders. For each sample configuration, five tests have been conducted to account for the material variability and allow an examination of testing repeatability. Individual tests in a generic (Ri) configuration are differentiated by adding their test name in the form of Cj, where j is simply the test number. The lateral confinement of particles is provided by rigid vertical walls fixed by a pair of front and rear transparent plexi plates. No contact between the face of the cylinders and the front and rear plexi plates exists and the rods are in a state of plane stress. The use of such a system implies no particle re-arrangement, however, owing to the compressibility of the material in the vertical direction, frictional forces may develop at the wall-particle side contacts.

The testing was conducted using a displacement controlled electro-mechanical loading frame (Figure 1b). The rod cylinders are compressed between two rigid steel plates: the top plate is fixed to the loading ram incorporating an LVDT for vertical displacement measurements and a 5 KN-load cell (with a linear response throughout the whole measurement range), while the lower platen moves upwards with a constant speed, fixed at 0.05 mm/min. During the crushing test, a piezoelectric AE sensor with a bandwidth between 10 kHz and 1 MHz records the acoustic emissions. While the AE sensor cannot be placed in direct contact with the material, the sensor was positioned beneath the sample within the steel base plate (Figure 1b), at a depth of about 1 cm, providing the closest possible option. The AE sensor was fixed via a mechanical system that ensured a constant holding force. Silicon grease was also used as a coupler. The AE signal produced by the piezoelectric sensor was conditioned by a 20 dB gain preamplifier before being routed to a 18bit A/D data acquisition system. The data acquisition unit can record AE signals at frequencies up to 40 MSamples/s. However, 1MS/s was considered sufficient to attain a 500kHz bandwidth of interest, while a sampling length of 5kSamples provided a window record time duration (5120 microseconds) enough to capture the full AE burst information.

During the test, the AE bursts (higher than an environmental laboratory detection threshold ranging from 36 to 40 dB) were recorded together with the resulting vertical force and vertical displacements. The set-up was completed by a video camera (25 frames/second rate) focusing on the front side of the sample and establishing the connection between the observed particle crushing patterns, force-displacement and AE activity. The use of an ordinary video recorder was meant to provide qualitative indication of the nature of the events and no additional image processing was conducted. While the synchronisation of the output parameters was not done automatically as an independent data acquisition unit was used for the force and displacement records, the sync error was sufficiently low not to affect the identification of the AE signals corresponding to various particle crushing events.

3. Results

3.1 General observations

Figures 2a-e show the force-displacement relationships for all the tests conducted on the sample configurations illustrated in Figure 1a. For R1 samples, the force increase in the initial stages of the loading takes place at a lower rate, suggesting either a softer response of the contacts or compliance in the loading system. Overall, the force-displacement is non-linear, marked by force fluctuations of small amplitude. The onset of these fluctuations corresponds well with the beginning of the material crushing in compression near the particle contact zones (Figure 3a) as also predicted by Tsoungui et al. (1999) for disks in biaxial compression. Ultimately, a sudden vertical splitting running through the cylinder length occurs in the central part of the chalk cylinder (test R1C3, Figure 3b), rendered also by a sharp drop of the reaction force. For these R1 tests, the loading is stopped at this point. Similar breakage mechanisms, local particle crushing and vertical splitting, are also observed for the chalk cylinders of the other samples R2-R5. These samples were sufficiently loaded to capture two or three major particle breakages and Figure 4 shows pictures of the side of selected tests at the onset of consecutive vertical particle splitting events. Although no quantitative assessment was conducted, from the video observations it was clearly inferred that while the splitting mechanisms are similar, the extent of the initial fracture varied from particle to particle with inherent variations of the corresponding AE features. No clear succession patterns of the broken particles from one test

to another (either within the same test configuration or between different test configurations) were observed. With some exceptions, when the breakage of particles succeeded at a relatively short interval, the second particle breakage was preceded by further fracture growth, extensive compression damage and additional crack developments of the previously crushed particle. The critical forces recorded at the crushing point and the corresponding displacements, respectively decrease and increase with the increase in the number of the chalk cylinders in the 2D samples R1 to R5. Figure 2f shows these tendencies for the first particle vertical splitting case.

3.2 Acoustic Emission

AE signals (hits) can be characterized by a range of discrete features. For simplicity, only the amplitude (maximum AE signal excursion during the AE hit), duration (the time from the first to the end of the last AE threshold crossings), and absolute energy (integral of the AE squared voltage signal divided by a reference resistance over the duration of the AE hit) are considered. Figure 5 displays the evolution of these AE features for representative R1-R5 samples (R1C3, R2C15, R3C27, R4C30 and R5C35 of which side views were also shown in Figures 3 and 4) combined with the mechanical response. The occurrence of the sudden vertical particle splitting as captured by the video camera and described by a sharp force drop is marked by a vertical arrow on the top graphs. Although the local particle crushing in compression at the particle-rigid plate (R1C3) and particle-particle (the other R2-R5 tests) contacts generate AE hits of relatively high duration, these are characterized by low AE amplitudes and energy. Contrary, for all the sample configurations, the vertical particle splitting systematically stands out with highest AE amplitudes and energy. The cumulated number of counts (for one AE hit, ‘counts’ represents the number of positive threshold crossings) showing sudden high slope gradients can also capture the rate of these AE occurrences. In between successive particle splitting events, the AE activity is sometimes particularly important due to the fracture growth and the occurrence of additional cracks of the previously damaged particle (R2C15). For some tests (R3C27, R5C35), more intense AE activity precedes the first major particle splitting event, while for others, the AE intensifies after the second and third major crushing events (R3C27 and R4C30, respectively). Overall, the variations of the AE response show quite a large range of scenarios and clearly expose the complexity of the interpretation even for a relatively simple particulate system.

Figure 6 presents the waveforms of the AE hits corresponding to the main splitting particle events for all the tests shown in Figure 5. The time axis in Figure 6 is relative to the beginning of the AE signal record. The strength (amplitude, energy) of AE signals corresponding to major particle splitting are dependent on the breakage intensities given by the extent of the fracture and associated energy release but it can also depend on the position of the particles relative to the AE sensor as waves produced further away from the sensor undergo damping while propagating through the granular system, possibly generating AE signals of lower amplitudes and energy. However, the weighting of these effects on the AE output is complex. For example, the maximum amplitude of the first split event of R4C30 is ten times lower than the maximum amplitude of R1C3, although the crushing occurs at the same location relative to the AE sensor (see also R3C27 and R5C35, 1st split), but similar maximum amplitudes of AE signals may occur for particles located at different positions relative to the AE sensor (1st split events for R1C3 and R3C27). For a given test, for example R3C27, the strength of the AE signals corresponding to the first and second particle breakages occurring in the top and bottom particles, respectively, seems not to be affected by the particle position relative to the AE sensor, while for R5C35 test, the strength of the AE signals corresponding to the crushing events of the middle particle and top particle are several order of magnitude apart. .

The analysis of the AE waveforms shown in Figure 6 corresponding to succesive particle splitting events for the samples with multiple cylinders is conducted in the frequency domain based on Welch's power spectral density estimate method (Welch, 1967) using the Hamming window option of the Matlab package (MATLAB 2010) and is presented in Figure 7. All AE signals exhibit multiple peaks in the amplitude-frequency domain mainly over 20 kHz to 50 kHz frequency range. For one sample configuration, although some peak amplitudes are bigger than others, the normalised power spectra density estimates of the AE signals corresponding to succesive particle splitting events present a very good match in terms of the peak frequencies, and this occurs irrespective of the position of the crushed particle, extent of the particle fracture and energy release. While these results can be considered as evidence of the existence of a typical AE signature for a typical particle crushing mechanism, its origin could also be a feature of the dynamic properties of the whole sample system which vibrates at its own resonant

frequencies (Alvarado and Coop, 2012, O'Donovan et al., 2016). From a simple inspection of the normalised power spectra results of the AE signals corresponding to the first crushing event of different sample configurations with multiple cylinders in Figure 8, a slight shift of the main peak frequencies towards the origin of the frequency axis is noticed when the number of cylinders is increased. More cylinders are added in a one column sample configuration, more flexible the system may be expected to be, hence lower resonant frequencies. However, comparison of all these spectra corresponding to the first major particle splitting event with the power spectra of the major particle splitting AE signal of R1C3 (single particle) also shown in Figure 8, provides interesting evidence of a relatively good match among the peak frequencies. Furthermore, in this normalised space, the power spectra of R1C3 appears as an envelope limit for the other sample configurations, with the best matching occurring for R4C30 sample where the position of both crushed particles is identical (bottom of the sample). An analytical estimation of the fundamental frequency of an unconfined chalk cylinder of similar diameter under top and bottom fixed kinematic constraints using a shear wave propagation velocity of about 600 m/s gives a value around 15 kHz, of a similar order of magnitude of the peak frequencies of the R1C3 AE signal. While the study of the direct free vibrations of a complete sample system configuration can be imagined, its application remains difficult in practice. As an alternative, numerical simulations are currently conducted to explore and infer the origin of the correspondence among these peak frequencies, systems' modes of vibration and the AE signature of the crushing mechanism.

4. Conclusions

A 2D analogue granular material formed of rod cylinders of chalk was tested under one-dimensional oedometric loading conditions. Passive non-destructive Acoustic Emission (AE) monitoring technique was employed to describe the occurrence of crushing of individual particles. The features of the recorded AE signals (amplitude and energy) corroborate well the observations based on video records of the exposed face of the 2D sample, as well as the vertical loading and displacement measurements of the global sample. While AE signals features can capture the particle crushing in 2D granular systems, their occurrence shows high complexities driven by internal crushing particle mechanisms and geometrical position of

particles with respect to the AE monitoring device. For a given sample configuration, the frequency content of AE signals shows some evidence of the existence of an AE signature for a typical particle crushing mechanism, but they may also be a consequence of the dynamic properties of the whole system. Further numerical analyses are currently performed to explore this latter point. Additional tests on more complex 2D samples are also being conducted.

Acknowledgements

The authors would like to acknowledge the University of Bristol and Prof Paul Wilcox for their support of the project. Dr Nicholas Alexander is acknowledged for fruitful discussions and suggestions for data analysis.

References

Alvarado G and Coop, MR (2012) On the performance of bender elements in triaxial tests. *Géotechnique*, **62(1)**: 1–17.

Aslan, H, and Baykal, G (2006). Analysing the crushing of granular materials by sound analysis technique. *Journal of Testing and Evaluation*, **34(6)**: 1-7.

Baud, P, Klein, E and Wong, TF (2004) Compaction localization in porous sandstone: spatial evolution of damage and acoustic emission activity. *Journal of Structural Geology*, **26**, 603-624.

Bohse J (2000) Acoustic emission characteristics of micro-failure processes in polymer blends and composites, *Composite Science and Technology*, **60**, 1213-1226.

Calvetti, F, Combe, G and Lanier, J (1997) Experimental micromechanical analysis of a 2D granular material: Relation between structure evolution and loading path. *Mechanics of Cohesive-Frictional Materials*, **2(2)**: 121–163.

Chichibu, A, Jo, K, Nakamura, M, Goto, T, and Kamata, M, (1989) Acoustic emission characteristics of unstable slopes, *Journal of Acoustic Emission*, Vol. **8**, 107–111.

Dai S and Labuz JF (1997) Damage and failure analysis of brittle materials by acoustic emission. *J Mater Civil Eng.*, **9(4)**: 200-205.

Dixon, N, Hill, R and Kavanagh, J, (2003) Acoustic emission monitoring of slope instability: Development of an active waveguide system, *Proceedings of the ICE: Geotechnical Engineering*, Vol. **156**, 83–95.

Dixon, N and Spriggs, M, (2007) Quantification of slope displacement rates using acoustic emission monitoring, *Canadian Geotechnical Journal*, Vol. **44**, 966–976.

Fernandes, F, Syahrial, AI and Valdes, JR (2010) Monitoring the oedometric compression of sands with acoustic emissions, *Geotechnical Testing Journal*, American Society for Testing and Materials, **33**, 410–415.

Geng, J and Behringer, RP (2005). Slow drag in two-dimensional granular media, *Physical Review E - Statistical, Nonlinear, and Soft Matter Physics*, **71(1)**, 1–19.

Giordano M, Calabro A, Esposito C, D'Amore A, and Nicolais L, (1998) An acoustic-emission characterization of the failure modes in polymer–composite materials, *Composite Science and Technology*, **58**, 1923-1928.

Haselbach W and Lauke B, (2003) Acoustic emission of debonding between fibre and matrix to evaluate local adhesion, *Composite Science and Technology*, **63(15)**: 2155-2162.

Huguet S, Godin N, Gaertner R, Salmon L and Villard D (2002) Use of acoustic emission to identify damage modes in glass fibre reinforced polyester, *Composite Science and Technology*, **62**, 1433–1444.

Hung, MH, Lauchle, GC and Wang, MC, (2009) Seepage-induced acoustic emission in granular soils, *J. Geotech. Geoenviron. Eng.,* **135**: 566–572. doi:10.1061/(ASCE)1090-0241(2009)135:4(566)

Ibraim, E, Lanier, J, Muir Wood, D and Viggiani G, (2010) Strain path controlled shear tests on an analogue granular material. *Géotechnique*, **60(7)**: 545 – 559.

Ibraim, E, Luo, S and Diambra, A, (2017) Particle soil crushing: passive detection and interpretation. *Proceedings of 19th ICSMGE*, Seoul, pp. 389-392.

Indraratna, B, Vinod, JS and Lackenby, J (2009) Influence of particle breakage on the resilient modulus of railway ballast. *Géotechnique*, **59(7)**: 643–646.

Ingraham, MD, Issen, KA and Holcomb, DJ, (2013) Use of acoustic emissions to investigate localization in high-porosity sandstone subjected to true triaxial stresses. *Acta Geotechnica*, **8(6)**: 645-663.

338 Karner, SL, Chester, FM, Kronenberg, AK and Chester, JS, (2003) Subcritical compaction and
339 yielding of granular quartz sand, *Tectonophysics* Vol.**377**, 357–381.
340 Koerner RM and Lord, AE Jr., (1974) Acoustic Emissions in Stressed Soil Samples. *The Journal*
341 *of the Acoustical Society of America,* **56**, 1924-1927; https://doi-
342 org.bris.idm.oclc.org/10.1121/1.1903538
343 Koerner, R, Lord, A, McCabe, W and Curran, J, (1976) Acoustic-emission behavior of granular
344 soils, *Journal of the Geotechnical Engineering Division – ASCE*, Vol.**103**, 1460–1461.
345 Koerner, RM, Lord, AE and McCabe, WM, (1977). Acoustic-emission behavior of cohesive soils,
346 Journal of the Geotechnical Engineering Division – ASCE, Vol.**103**, 837–850.
347 Kuwajima, K, Hyodo, M, and Hyde, AFL, (2009) Pile Bearing Capacity Factors and Soil
348 Crushability, *J. Geotech. Geoenvironmental. Eng*., **135(7)**, 901–913.
349 Lackenby, J, Indraratna, B, McDowel, G and Christie, D, (2007). Effect of confining pressure on
350 ballast degradation and deformation under cyclic triaxial loading, *Geotechnique*, **57(6)**: 527-
351 536.
352 Liu, E (2010) Breakage and deformation mechanisms of crushable granular materials.
353 *Computers and Geotechnics*, **37(5)**: 723-730.
354 Lord, AE and Koerner, RM, (1974) Acoustic-emission response of dry soils. *Journal of Testing*
355 *and Evaluation,* **2**, 159–162.
356 Lord, AE Jr. and Koerner, RM (1975) Acoustic Emissions in Soils and Their Use in Assessing
357 Earth Dam Stability. *The Journal of the Acoustical Society of America*, **57**, 516-519
358 https://doi-org.bris.idm.oclc.org/10.1121/1.2033173
359 Luo, S, Diambra, A, and Ibraim, E (2016)a Application of Acoustic Emission on Crushing
360 Monitoring of Individual Soil Particles in Uniaxial Compression Test. *In Proc. of 32nd*
361 *ECAET*: Prague, Czech Republic, September, pp. 305-313.
362 Luo, S, Diambra, A and Ibraim, E (2016)b Particle crushing: passive detection. 1st IMEKO TC-4.
363 *Int. Workshop on Metrology for Geotechnics*. Benevento, Italy, March
364 Luo, S, Ibraim, E and Diambra, A (2018) The interpretation of soil particle crushing by Acoustic
365 Emission Method. *International Symposium on Geo-Mechanics from Micro to Macro*, Altanta,
366 USA, 6 p.
367 MATLAB - The language of technical computing, 7 ed: The Mathworks Inc, 2010

Mao, WW and Towhata, I (2015) Monitoring of single-particle fragmentation process under static loading using acoustic emission. *Applied Acoustics*, **94**, 39-45.

Michlmayr, G and Or, D, (2014) Mechanisms for acoustic emissions generation during granular shearing. *Granular Matter*, **16**:627–640. doi:10.1007/s10035-014-0516-2

Misra, A and Poorsolhjouy, P (2013) Micro-macro scale instability in 2D regular granular assemblies, *Continuum Mechanics and Thermodynamics*, **27(1-2)**: 63–82.

Mogami, T (1965). A statistical approach to the mechanics of granular materials, Soils and Foundations, 5(2), 26-36

Muir Wood, D (2007) The magic of sands — The 20th Bjerrum Lecture presented in Oslo, 25 November 2005. *Canadian Geotechnical Journal*, **44(11)**: 1329–1350. http://doi.org/10.1139/T07-060

O'Donovan, J, Ibraim, E, O'Sullivan, C, Hamlin, S, Muir Wood, D and Marketos, G, (2016) Micromechanics of seismic wave propagation in granular materials. *Granular Matter***, 18: 56**. https://doi.org/10.1007/s10035-015-0599-4

Shigeishi, M, Colombo, S, Broughton, KJ, Rutledge, H, Batchelor, AJ and Forde, MC, (2001), Acoustic emission to assess and monitor the integrity of bridges. *Construction and Building Materials*, **15**, 35-49.

Smith, A, Dixon, N, Meldrum, P, Haslam, E., and Chambers J. (2014) Acoustic emission monitoring of a soil slope: Comparisons with continuous deformation measurements. *Géotechnique Letters*, **4:4**: 255-261.

Stojanova, M, Santucci, S, Vanel, L and Ramos, O (2014) High Frequency Monitoring Reveals Aftershocks in Subcritical Crack Growth. *Physical Review letters*, **112(11)**: 115502

Takei, M, Kusakabe, O and Hayashi, T (2001) Time-dependent behavior of crushable materials in one-dimensional compression tests. *Soils and Foundations*, **41(1)**: 97–121.

Tanimoto, K and Nakamura, J (1981) Studies of acoustic emission in soil. In: Drnevich, V.P., Gray, R.E. (Eds.), *Acoustic Emission in Geotechnical Engineering Practice*, ASTM STP 750, 164–173

Tanimoto, K and Tanaka, Y, (1986) Yielding of soil as determined by acoustic emission. *Soils and Foundations*, **26(3)**: 69-80

Tsoungui, O, Vallet, D, and Charmet, J-C (1999) Numerical model of crushing of grains inside two-dimensional granular materials. *Powder Technology*. **105**: 190-198. 10.1016/S0032-5910(99)00137-0.

Wan, R, Guo, P. and Al-Mamun, M (2005) Behaviour of granular material materials in relation to their fabric dependencies. *Soils and Foundations*, **45(2)**: 77-86.

Wang, Y, Ma, C and Yan, W, (2009). "Characterizing bond breakages in cemented sands using a mems accelerometer", *Geotechnical Testing Journal*, Vol.**32**, 1–10.

Welch, PD (1967) The Use of Fast Fourier Transform for the Estimation of Power Spectra: A Method Based on Time Averaging Over Short, Modified Periodograms. *IEEE Transactions on audio and electroacoustics*, AU-15, No. 2

White, DJ and Bolton, MD (2004) Displacement and strain paths during plane-strain model pile installation in sand. *Geotechnique*, **54(6)**: 375–397.

Yuyama S, Okamoto, T and Nagataki, S (1994). Acoustic emission evaluation of structural integrity in repaired reinforced concrete beams, *Material Evaluation*, **52(1)**: 88-90.

Young, P and Martin, CD, (1993) Potential Role of Acoustic Emission/Microseismicity Investigations in the Site Characterization and Performance Monitoring of Nuclear Waste Repositories. *International Journal of Rock Mechanics and Mining Science & Geomechanics Abstracts*, **30(7)**: 797-803.

Zhang, J, Wong, TF, Yanagidani, T and Davis, DM (1990) Pressure-induced microcracking and grain crushing in Berea and Boise sandstones: acoustic emission and quantitative microscopy measurements. *Mechanics of Materials*, **9**, 1-15.

Figure captions

Figure 1. (a) Side view of the 2D samples; R1 to R5 represent their generic name; (b) schematic view of the loading set up including the loading frame, the sample, video camera, AE sensor, force and displacement transducers.

Figure 2. (a) to (e): force – displacement for different sample configurations including repeatability; (f): force and displacement corresponding to the first major particle splitting event for each sample configuration from R1 to R5.

Figure 3. Views of (a) local crushing of the chalk cylinder at the particle – platen contact, and (b) just at the moment of vertical particle splitting taken during the one-dimensional tests on R1C3 sample.

Figure 4. Successive pictures at the onset of the particle splitting events taken during one-dimensional tests on: (a) R2C15; (b) R3C27; (c) R4C30; (d) R5C35 samples.

Figure 5. Acoustic emission data in terms of the amplitude, duration, absolute energy and cumulated counts of the recorded AE signals, during the during one-dimensional tests on the selected R1C3, R2C15, R3C27, R4C30 and R5C35 samples.

Figure 6. AE waveforms recorded at the vertical splitting moment of the particles in successive order for the selected tests R1C3, R2C15, R3C27, R4C30 and R5C35. The position of the crushed particles is also shown on the right of each graph. The curves in the first column correspond to the first major vertical particle splitting (red particle). The second column refers to the second splitting event occurring on a different particle (blue particle). Only the sample R4C30 experienced a third vertical splitting event (black particle). Please note the change of the waveform amplitude limits from one test to another.

Figure 7. Power spectra of successive AE signals shown in Figure 6 corresponding to the vertical particle splitting events during the tests: (a) R2C15; (b) R3C27; (c) R4C30; (d) R5C35. The position of the crushed particles following a similar colour code is also presented in each graph.

Figure 8. Comparison of power spectra of AE signals corresponding to the particle vertical splitting of single confined cylinder, test R1C3, and the first particle vertical splitting of: (a) R2C15; (b) R3C27; (c) R4C30; (d) R5C35 tests. The position of the crushed particle for the latter tests is also shown in each graph.

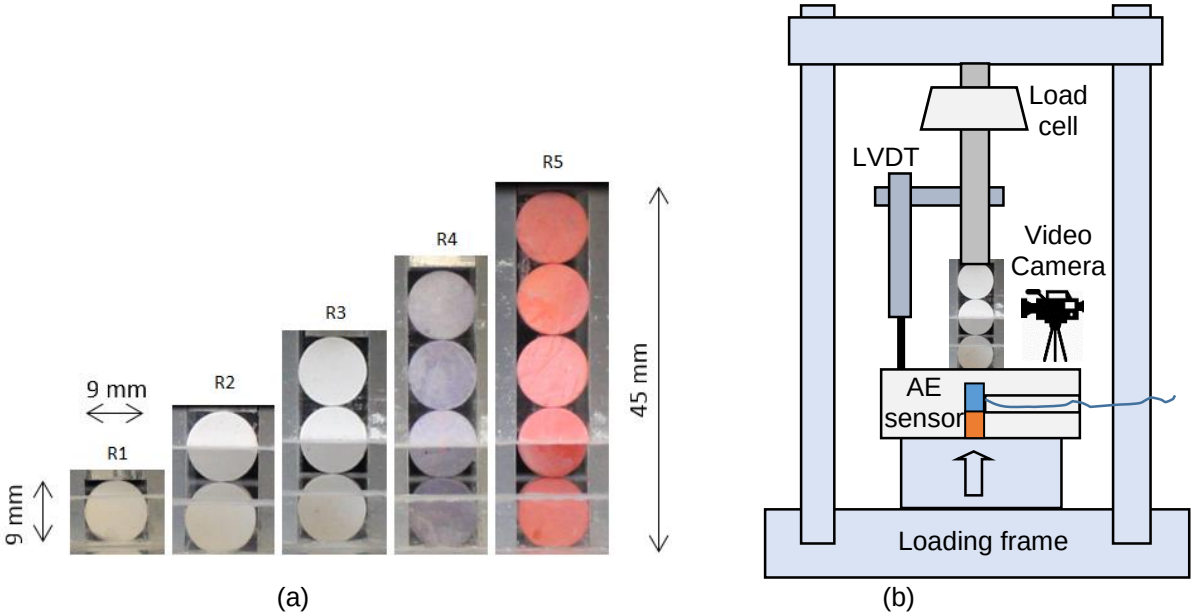

Figure 1. (a) Side view of the 2D samples; R1 to R5 represent their generic name; (b) schematic view of the loading set up including the loading frame, the sample, video camera, AE sensor, force and displacement transducers.

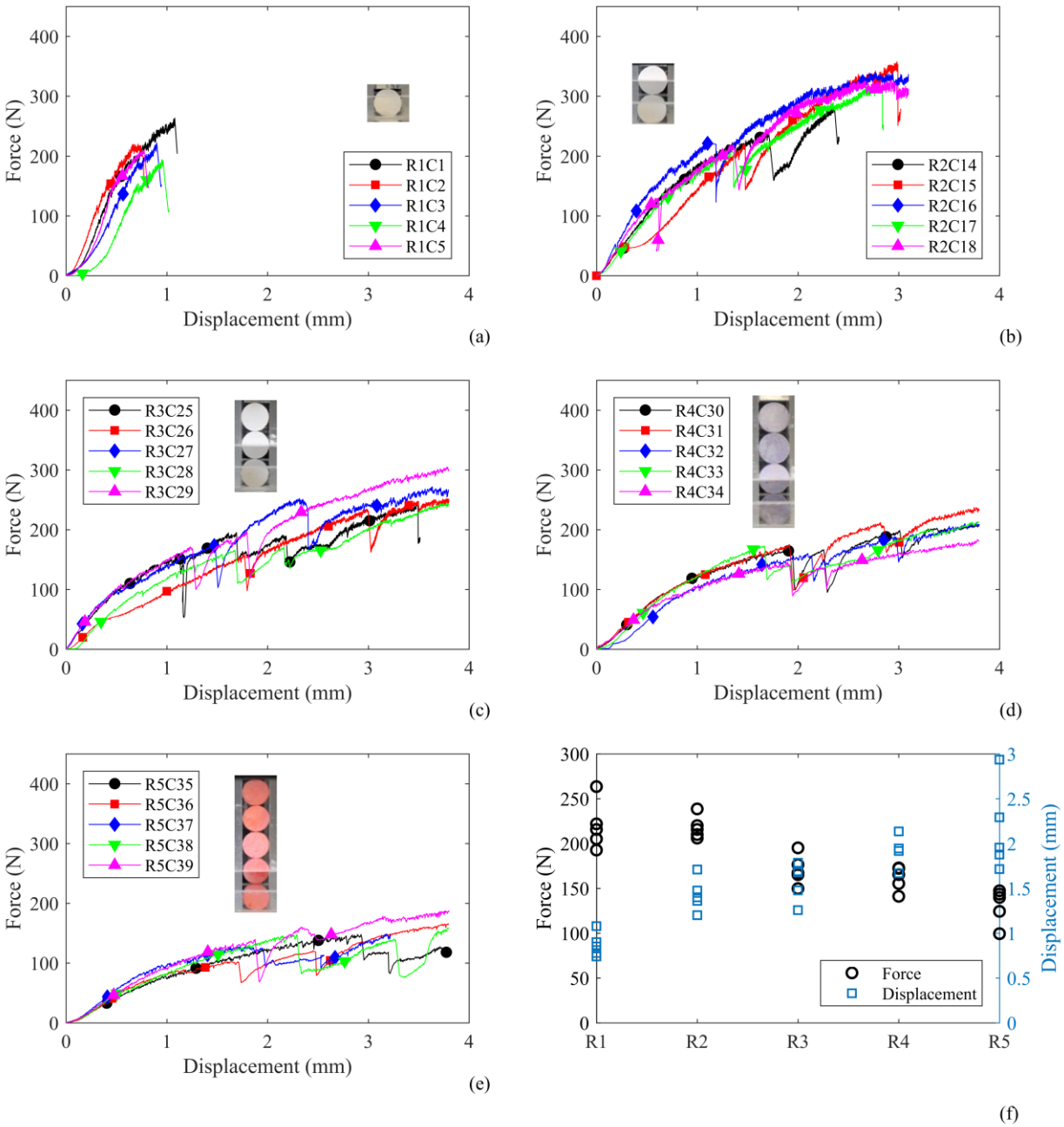

Figure 2. (a) to (e): force – displacement for different sample configurations including repeatability; (f): force and displacement corresponding to the first major particle splitting event for each sample configuration from R1 to R5.

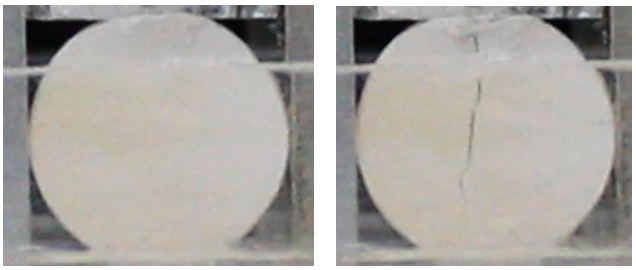

(a) (b)

Figure 3. Views of (a) local crushing of the chalk cylinder at the particle – platen contact, and (b) just at the moment of vertical particle splitting taken during the one-dimensional tests on R1C3 sample.

(a) (b)

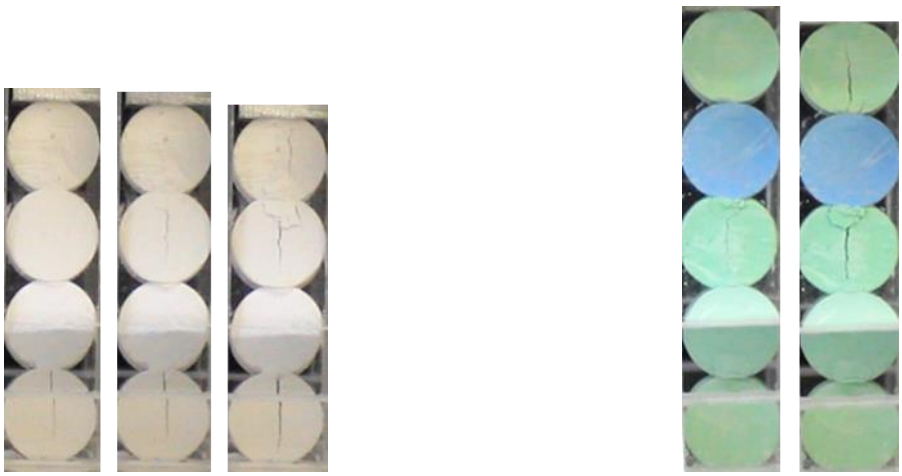

(c) (d)

Figure 4. Successive pictures at the onset of the particle splitting events taken during one-dimensional tests on: (a) R2C15; (b) R3C27; (c) R4C30; (d) R5C35 samples.

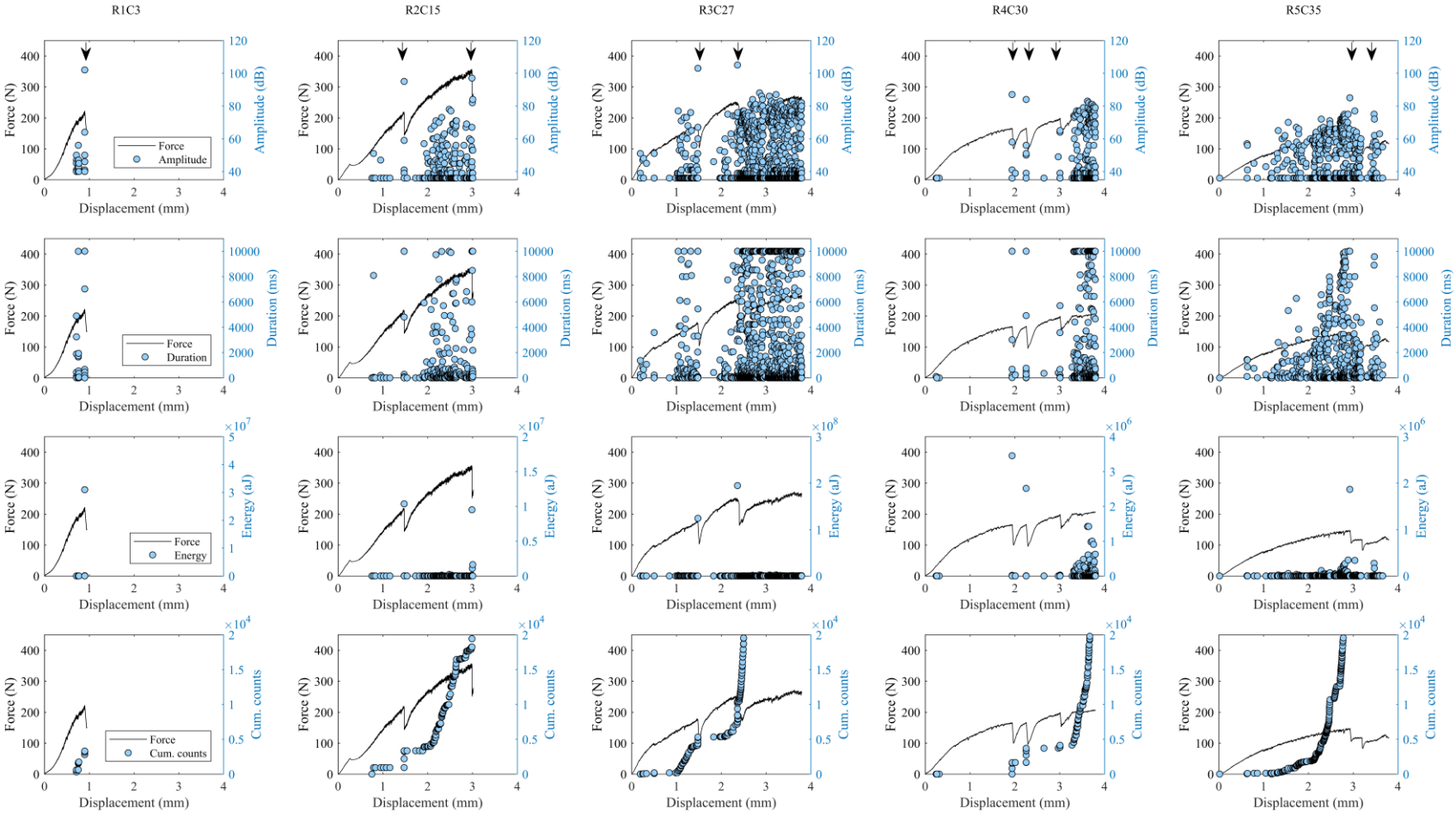

Figure 5. Acoustic emission data in terms of the amplitude, duration, absolute energy and cumulated counts of the recorded AE signals, during the during one-dimensional tests on the selected R1C3, R2C15, R3C27, R4C30 and R5C35 samples.

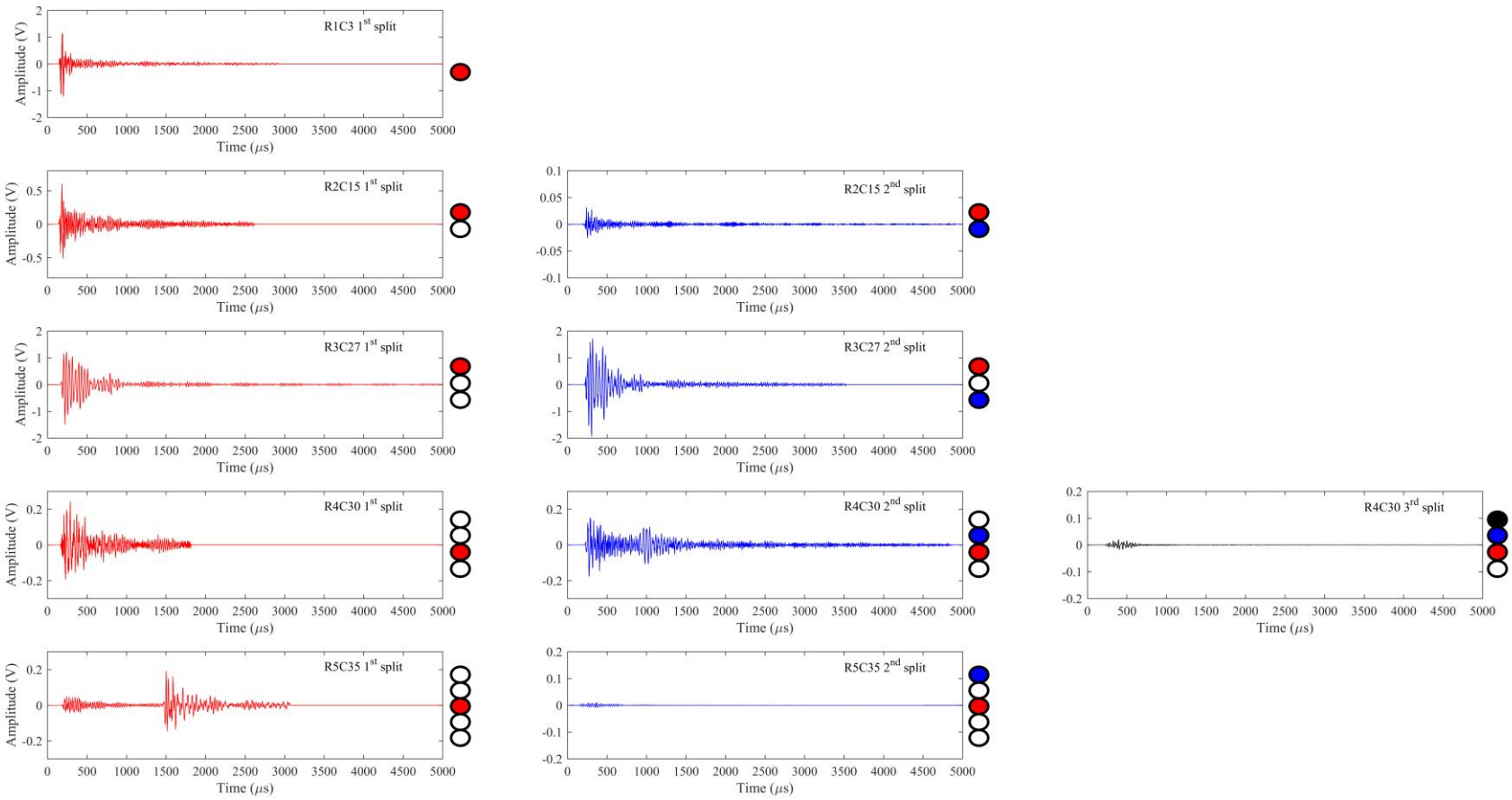

Figure 6. AE waveforms recorded at the vertical splitting moment of the particles in successive order for the selected tests R1C3, R2C15, R3C27, R4C30 and R5C35. The position of the crushed particles is also shown on the right of each graph. The curves in the first column correspond to the first major vertical particle splitting (red particle). The second column refers to the second splitting event occurring on a different particle (blue particle). Only the sample R4C30 experienced a third vertical splitting event (black particle). Please note the change of the waveform amplitude limits from one test to another.

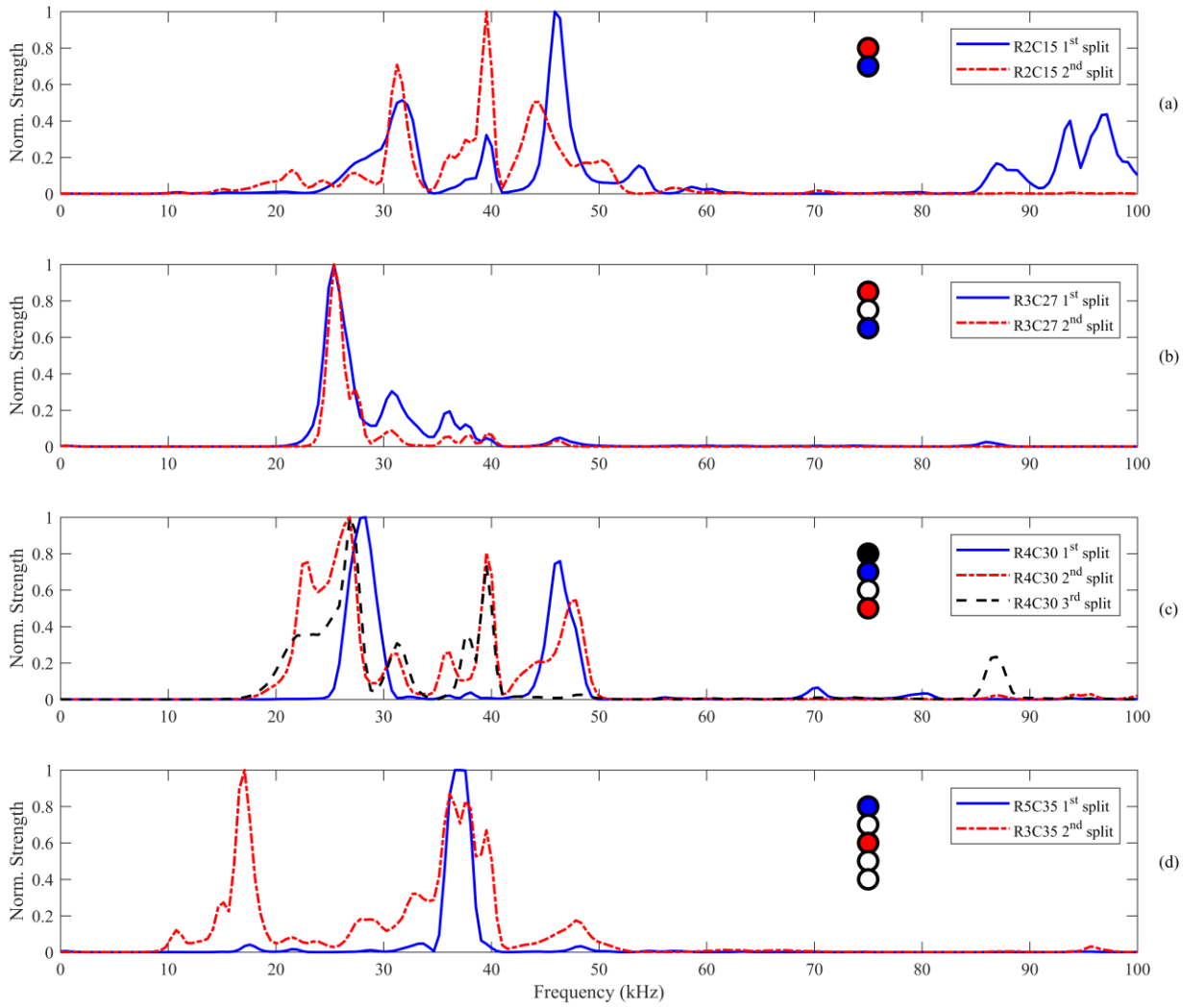

Figure 7. Power spectra of successive AE signals shown in Figure 6 corresponding to the vertical particle splitting events during the tests: (a) R2C15; (b) R3C27; (c) R4C30; (d) R5C35. The position of the crushed particles following a similar colour code is also presented in each graph.

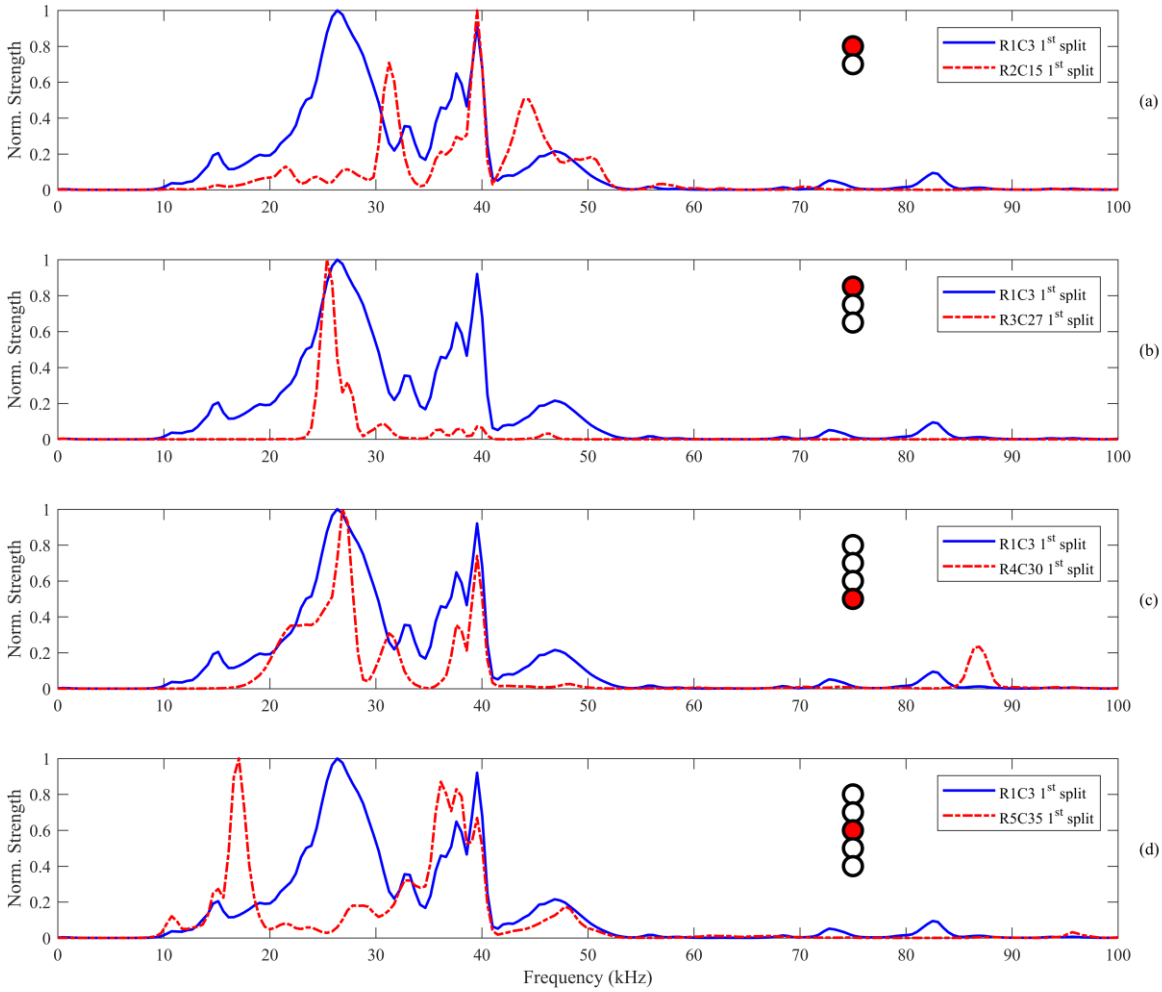

Figure 8. Comparison of power spectra of AE signals corresponding to the particle vertical splitting of single confined cylinder, test R1C3, and the first particle vertical splitting of: (a) R2C15; (b) R3C27; (c) R4C30; (d) R5C35 tests. The position of the crushed particle for the latter tests is also shown in each graph.